CHEMISTRY
A EUROPEAN JOURNAL

ChemPubSoc
Europe

DOI: 10.1002/chem.201301572

Synthesis of 3,3-Disubstituted Oxindoles by Palladium-Catalyzed Asymmetric Intramolecular α-Arylation of Amides: Reaction Development and Mechanistic Studies

Dmitry Katayev,[a] Yi-Xia Jia,[a, c] Akhilesh K. Sharma,[b] Dipshikha Banerjee,[a] Céline Besnard,[a] Raghavan B. Sunoj,*[b] and E. Peter Kündig*[a]

Abstract: Palladium complexes incorporating chiral N-heterocyclic carbene (NHC) ligands catalyze the asymmetric intramolecular α-arylation of amides producing 3,3-disubstituted oxindoles. Comprehensive DFT studies have been performed to gain insight into the mechanism of this transformation. Oxidative addition is shown to be rate-determining and reductive elimination to be enantioselectivity-determining. The synthesis of seven new NHC ligands is detailed and their performance is compared. One of them, **L8**, containing a *t*Bu and a 1-naphthyl group at the stereogenic centre, proved superior and was very efficient in the asymmetric synthesis of fifteen new spiro-oxindoles and three azaspiro-oxindoles often in high yields (up to 99%) and enantioselectivities (up to 97% *ee*; *ee* = enantiomeric excess). Three palladacycle intermediates resulting from the oxidative addition of [Pd(NHC)] into the aryl halide bond were isolated and structurally characterized (X-ray). Using these intermediates as catalysts showed alkene additives to play an important role in increasing turnover number and frequency.

Keywords: arylation · asymmetric catalysis · N-heterocyclic carbenes · oxindoles · palladium

Introduction

The oxindole motif is found in a large number of natural products and synthetic analogues with a wide array of biological activities.[1] The intense interest in these heterocycles is also manifest by the frequent reviews dedicated to aspects of oxindole synthesis.[1d,e 2] Many of these compounds incorporate a stereogenic center at C(3). Consequently much activity has focused on the synthesis of enantiomerically enriched compounds of this family. One route of access is by modification of a pre-existing ring system—typically either a simpler oxindole or an isatin. Recent examples include enantioselective nucleophilic addition to isatins,[3] direct functionalization of 3-substituted oxindoles by alkylation or arylation,[4] fluorination,[5] hydroxylation,[6] aldol reaction,[7] Mannich reaction,[8] Michael addition,[9] amination,[10] and arylation[11] reactions.

Alternatively, the stereogenic center can be formed during cyclization of an acyclic precursor. Pioneering elegant work here stems from the Overman group[12] who have developed an enantioselective intramolecular Mizoroki–Heck reaction for this transformation. An example detailing the formation of a spiro-oxindole is shown in Scheme 1. Zhu extended these studies by an asymmetric tandem Heck-cyanation reaction.[13]

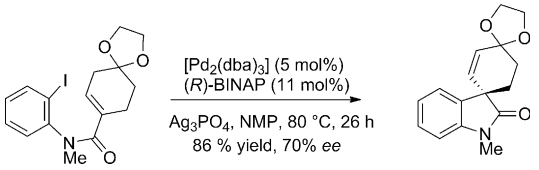

Scheme 1. Spiro-oxindole synthesis by asymmetric Heck cyclization.[12] BINAP = 2,2′-bis(diphenylphosphino)-1,1′-binaphthyl.

In 2001, Hartwig and co-workers reported the results of an extensive study of the Pd^0-catalyzed intramolecular α-arylation of anilides to give 3,3-disubstituted oxindoles (Scheme 2).[14] This included a large number of chiral ligands. Chiral bidentate phosphine ligands generally afforded products with poor asymmetric induction. The most promising ligands were bulky chiral N-heterocyclic carbenes

[a] Dr. D. Katayev, Prof. Y.-X. Jia, Dr. D. Banerjee, Dr. C. Besnard, Prof. E. P. Kündig
Department of Organic Chemistry, University of Geneva
30 Quai Ernest Ansermet, 1211 Geneva 4 (Switzerland)
Fax: (+41) 22-379-3215
E-mail: peter.kundig@unige.ch

[b] A. K. Sharma, Prof. R. B. Sunoj
Department of Chemistry, Indian Institute of Technology Bombay
Powai, Mumbai 400076 (India)
Fax: (+22) 2576-7151
E-mail: sunoj@chem.iitb.ac.in

[c] Prof. Y.-X. Jia
Present address:
Zhejiang University of Technology
State Key Laboratory Breeding Base of
Green Chemistry-Synthesis Technology
Chaowang Road 18, Hangzhou, 310014 (P. R. China)

Supporting information for this article is available on the WWW under http://dx.doi.org/10.1002/chem.201301572.

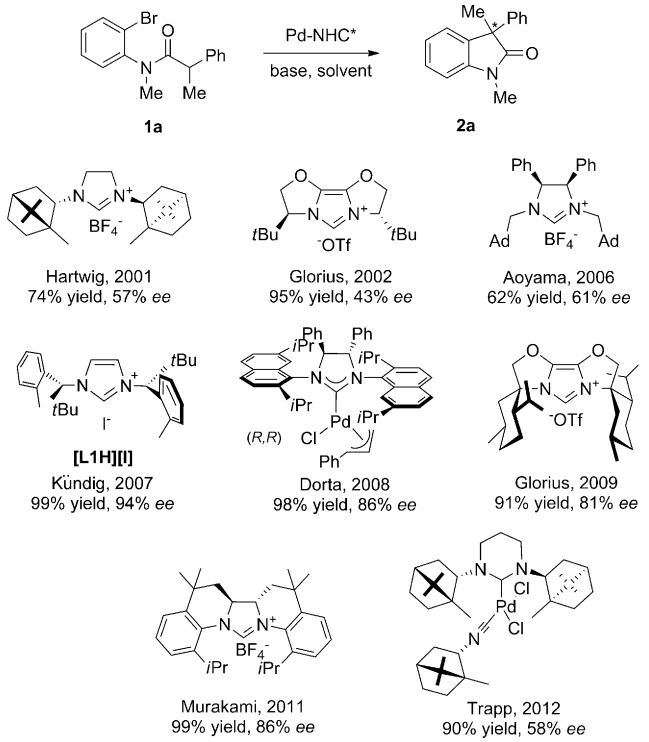

Scheme 2. Progress in the Pd-catalyzed asymmetric intramolecular arylation of amides by using chiral NHC ligands.

(NHC) though the results left much room for improvement. This study was followed by those of the groups of Glorius[15a] and Aoyama[15b,c] but only moderate enantioselectivities were obtained. The breakthrough in this area came in 2007 with the development of new chiral NHC ligands[15d,e] and both high yields and asymmetric induction were achieved in this approach to oxindoles. The main features of these ligands are bulky *t*Bu groups at the stereogenic centers α to nitrogen and *ortho*-substituents on the aromatic groups. Modification of the ligand aryl groups also gave access to highly enantioenriched oxindoles bearing heteroatoms at the oxindole stereogenic center (O and N).[15f] Since then, this chemistry has been expanded further[15g] and a number of other chiral carbene ligands have been reported to give excellent results (Scheme 2). Dorta developed new NHC ligands with a chiral N-heterocycle and naphthyl side chains and successfully applied palladium complexes incorporating these ligands in 3-alkyl-3-aryl,[15h] 3-allyl-3-aryl,[15i] and recently 3-flouro-3-aryl[15j] oxindole synthesis. Importantly, the initial drawback of having to separate stereoisomers of the Pd catalyst has now been overcome.[15k] Conformationally restricted chiral ligands developed by Glorius[15l] and Murakami[15m] also showed high asymmetric induction in this reaction, whereas a catalyst with a six-membered NHC ligand did not reach the same level of asymmetric induction.[15l]

We argued that in the ligand family reported from this laboratory, minimization of allylic strain places the catalysts stereodirecting aryl planes into the appropriate space. Hence, minimization of allylic strain plays a similar role in these chiral monodentate ligands as the chiral backbone in bidentate chiral ligands. The entropic advantage of the bidentate phosphorous ligands is compensated by the robust metal–NH–carbene bond. This hypothesis was strengthened by X-ray crystal structures of a Pd^{II}–NHC complex[15e] and of a number of NHC–borane and NHC–gold complexes.[16] More recently these ligands also have found application in the Pd-catalyzed intramolecular coupling reactions between aryl bromides and unactivated methylene groups leading to the 2-substituted and 2,3-disubstituted indolines with high asymmetric induction.[17] A monodentate ligand proved essential in that reaction.

In our previous studies of the transformation of **1a**→**2a**, we used an in situ procedure to generate the catalysts. Thus, generation of [Pd^0(**L1**)] involved treating a mixture of [Pd_2(dba)$_2$] (dba = dibenzylideneacetone, 1,5-diphenyl-1,4-pentadion-3-one) and the imidazolium iodide [(*S*,*S*)-**L1**H][I] in dimethoxyethane with *t*BuONa. Hartwig and co-workers proposed a catalytic cycle analogous to that shown in Scheme 3

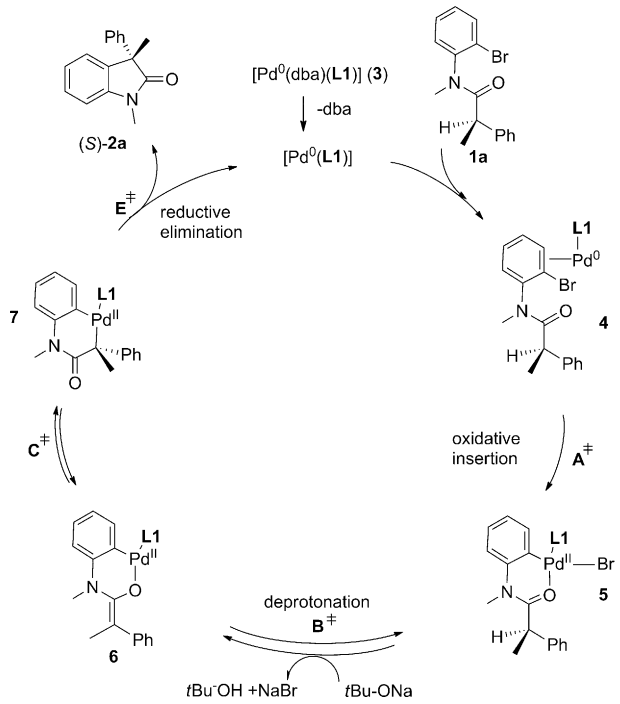

Scheme 3. Energetically most preferred mechanistic pathway for Pd–NHC*-catalyzed synthesis of oxindole (*S*)-**2a**.

and they isolated and analytically and spectroscopically characterized palladacycle **5**. These authors also established the oxidative addition step to be rate-determining. Structural and energetic information of the key intermediates was not available, however, and the step in which asymmetric induction occurs remained unknown.

In the present article we probe the mechanism of the intramolecular arylation of amides by a detailed DFT investigation and report the synthesis of new chiral NHC ligands, one of them showing strongly improved performance in catalysis leading to spiro-oxindoles. We also describe the isola-

tion and structural characterization of palladacycle intermediates and their use as catalysts in this reaction.

Results and Discussion

DFT investigations: A number of different mechanistic scenarios were examined for the [Pd^0(**L1**)]-catalyzed oxindole formation. Here, we focus only on the energetically most preferred pathway (Scheme 3). Alternative possibilities that differ in terms of the geometries of the palladacycle or in the mode and timing of bromide loss from various intermediates are detailed in the Supporting Information. Very recently, Curran and co-workers analyzed the implications of atropisomers of *N*-methyl-*N*-bromoarylacetamides and their Pd insertion products in this reaction sequence. Their study revealed isomerization to be rapid relative to the forward reaction. Cyclization to oxindoles is thus preceded by a dynamic kinetic resolution at an early stage of the reaction.[18]

The reaction is envisaged to begin with the formation of [Pd^0(dba)(**L1**)] (**3**) complex from [Pd^0(dba)$_2$] (Figure 4). The energy of 3 is taken as the reference for comparisons. The

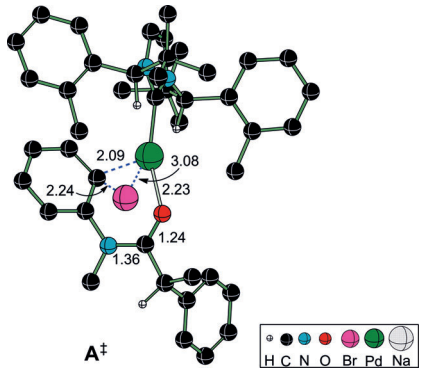

Figure 1. Optimized geometry of transition-state **A**‡.

catalytic cycle starts with the loss of dba from **3** and formation of a catalyst–substrate complex involving a Pd-η^2 arene bond (**4**). Oxidative addition follows next to provide palladacycle **5**. In the absence of additional base, **5** can be isolated. Hartwig and co-workers reported NMR spectroscopic data with tricyclohexylphosphine (PCy_3) as the ligand and, as will be shown later, we have isolated and structurally characterized palladacycles **5** incorporating chiral NHC ligands.

In the next step of the catalytic cycle, *t*BuONa abstracts the benzylic proton leading to the Pd-O-enolate **6**.[19] This is followed by isomerization to Pd-C-enolate **7**. Reductive elimination furnishes the final product and regenerates the [Pd^0(**L1**)] catalyst. In the next level of detail, features of the catalytic cycle, such as the formation of two diastereomeric palladacycles **5** from the racemic substrate, the role of base, the formation of the *E* or the *Z*-enolate, and the asymmetric induction provided by the ligand is addressed.

Enantioselectivity could be controlled by any of the three steps: 1) the substrate benzylic deprotonation leading to *E* or *Z* enolates, 2) the conversion of O-enolate to C-enolate, or 3) reductive elimination from the palladacycle leading to the oxindole product. DFT(B3LYP) computation was employed to identify the transition states (TSs) in an effort to delineate the factors contributing to enantioselectivity as well as to recognize the most likely step(s) responsible for asymmetric induction. The effect of solvent continuum is taken into account by computing energies by using 1,4-dioxane as the solvent. The discussion in the manuscript is based on the SMD$_{1,4\text{-dioxane}}$/B3LYP/6-311+G**(C,H,N,O,Na,Br), LANL2TZ(f)(Pd)/B3LYP/6-31G*(C,H,N,O,Na,Br); LANL2DZ(Pd) energies. The mechanisms emanating from both *R* and *S* enantiomers of the racemic substrate were considered. The energy difference between the diastereomeric transition states for the oxidative addition of [Pd(**L1**)] to (*R*)-**1a** and (*S*)-**1a** is only 1.0 kcal mol^{-1}, in favor of the *S* enantiomer. This leads to the two diastereomeric intermediates (*S,S,S*)-**5** and (*S,S,R*)-**5**. The optimized geometry of the oxidative addition transition state **A**‡ (for the *R* configuration) is shown in Figure 1.[20] As will be shown later, the two diastereomeric intermediates corresponding to **5** were isolated (as iodo-palladacycles) and structurally characterized.

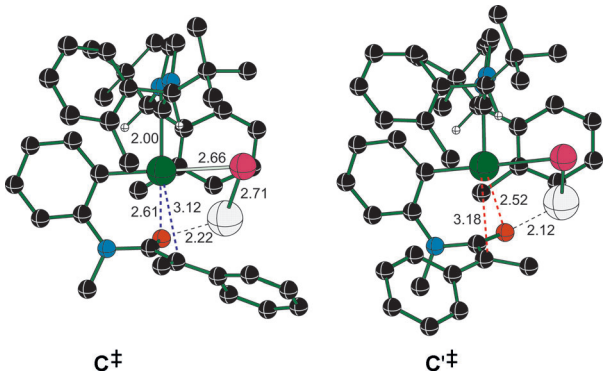

Figure 2. Preferred torsional transition states involved in the conversion of O-enolate to C-enolate. **C**‡ and **C′**‡ represent the conversion of *Z*- and *E*-O-enolates to C-enolates, respectively.

The next step is the deprotonation of **5** leading to palladium *O*-enolates **6**. For convenience to the reader we will leave out the descriptors for the ligand chirality as this will remain unchanged. The key features of the computed energetics can be gathered from the Gibbs free energy profile as given in Figure 4. The barrier for deprotonation of diastereomer (*S*)-**5** is 5.4 kcal mol^{-1}, whereas that for (*R*)-**5** it is 4.6 kcal mol^{-1}.[21] The computed energetics further indicate that (*R*)-**5** preferably leads to the *Z*-enolate, whereas (*S*)-**5** can result in both *E* and *Z*-enolate. The step leading to the generation of the enolate intermediate is not expected to be significant in the eventual enantioselectivity of this reaction.

A key point to note is a likely accumulation of the energetically more favored *Z*-O-enolate due to the equilibrium

between intermediates **5** and **6** connected by transition state **B**. Further, the barrier for *E*/*Z* conversion (within O-enolate) by rotation around the C=C bond is lower than those of the forward reactions. The next major event in the catalytic cycle is the transition from O-enolate **6** to C-enolate **7**. The barrier for rotation of the *Z*-O-enolate to (*R*)-**7** is found to be 0.9 kcal mol^{-1} lower than that for the *Z*-O-enolate to (*S*)-**7**. This step can influence the stereochemical outcome of the reaction. The *E*-enolate will give rise to palladacycle (*S*)-**7**, which will eventually lead to *R*-oxindole. The *Z*-O-enolate on the other hand, will convert to (*R*)-**7** and then to (*S*)-oxindole. Hence, different geometric isomers of **6** will lead to different enantiomers if the interconversion between *E* and *Z*-enolates is prevented. The optimized geometries of these transition states are provided in Figure 2 (TS **C**).[22]

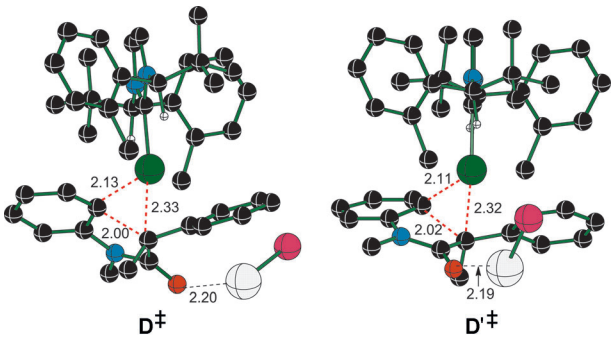

Figure 3. Optimized geometries of transition states for the reductive elimination leading to oxindole formation. $\mathbf{D}^{\ddagger}$ and $\mathbf{D'}^{\ddagger}$ are diastereomeric transition states leading to (*S*)-**2a** and (*R*)-**2a** products, respectively.

The structural features indicate the involvement of an early transition state wherein the incipient bond length between Pd and the new chiral center is much longer. It is further evident from the transition-state geometries that the new benzylic stereogenic centers in the two transition states are stereochemically distinct.

Finally, a reductive elimination leads to the product oxindole. The configuration at the benzylic carbon atom gets carried forward to the product as the reductive elimination is identified to be a concerted process with no additional intermediates. The stereochemistry of product oxindole, therefore, depends on the configuration as rendered in the previous step. The intermediate (*R*)-**7**, therefore, corresponds to the formation of oxindole (*S*)-**2a**, whereas (*S*)-**7** yields (*R*)-**2a**. The energy barrier for the reductive elimination in (*R*)-**7** to (*S*)-**2a** is 4.2 kcal mol^{-1} lower in energy than the corresponding conversion of (*S*)-**7** to (*R*)-**2a**. Hence, the transition state for formation of the (*S*)-oxindole is more favorable.[23] This prediction is in concert with the experimental observations.

The different transition states for the stereoselective reductive elimination leading to oxindole formation is examined. These transition states differ in the orientation and in terms of the prochiral faces of the substrate involved in the bond formation. Transition states $\mathbf{D}^{\ddagger}$ and $\mathbf{D'}^{\ddagger}$, in which the phenyl group of the substrate is positioned towards the catalyst, are found to be of lower energy (Figure 3). A favorable interaction between the substrate phenyl ring and palladium is noticed in both $\mathbf{D}^{\ddagger}$ and $\mathbf{D'}^{\ddagger}$. The chiral NHC side chain bearing *tert*-butyl and 2-methylphenyl groups is identified to provide differential steric environments to the substrate in the ring-closing step. Upon analysis of these transition states with the help of an *activation strain model*, it became evident that transition state $\mathbf{D'}^{\ddagger}$ suffers from higher steric-induced strain. The origin of increased strain has been traced to the closer proximity between the 2-methylphenyl arm of the catalyst and the phenyl and methyl substituents on the developing oxindole ring. Detailed geometric analysis of the transition state is provided in the Supporting Information.[24] When the oxindole ring is closer to the *tert*-butyl group of NHC, as in transition state $\mathbf{D}^{\ddagger}$, the distortion and proportionately the energy is found to be lower.[25]

In summary, the analysis of the Gibbs free energy profile (Figure 4) reveals that oxidative addition is the rate-limiting step leading to the formation of a stable intermediate **5**. The transition state for the reductive elimination presents the next-highest activation barrier (23.5 kcal mol^{-1}) to give the oxindole product (**2a**). The intermediates **6** and **7**, representing the 'black' pathway and ultimately leading to (*S*)-**2a** are lower in energy than those leading to (*R*)-**2a** and intermediates likely accumulate here. The energy barrier to (*S*)-**2a** from the lowest energy intermediate **7** thus favors the formation of (*S*)-**2a**.

New chiral NHC ligands: As previously stated, we presume that the ligand's aryl *ortho*-substituent fixes the orientation of the aryl ring in space through minimization of allylic strain. If correct, the substitution of the *ortho*-Me group by a fused aromatic ring could improve the ligand's performance.[15d–f] We have, therefore, extended this family of chiral NHC ligands to the naphthyl ligands **L8**–**L11** (Scheme 4). In preliminary communications we have shown that **L8** is the best performer in an intramolecular asymmetric Ar-Br/C-(sp^3)-H coupling reaction leading to indolines.[17] The excellent performance was linked to the high thermal stability of the Pd–**L8** bond. The X-ray structure of (*S,S*)-**L8**-BH_3 was also reported very recently.[16] We now detail the synthesis of the naphthyl imidazolium and dihydroimidazolium salts [**L8**H][I]–[**L11**H][I] and of the C_1-symmetric ligand precursors [**L12**H][BF_4]–[**L14**H][BF_4].

The syntheses of enantiopure amines **8** and **9** are shown in Scheme 5. Alkylation of the corresponding napthonitriles with *t*BuMgCl in the presence of a catalytic amount of CuBr followed by in situ reduction with $NaBH_4$ afforded (*rac*)-**8** and (*rac*)-**9** in good yields.

Amine (*rac*)-**8** was resolved by forming the diastereoisomeric salt with (L)-malic acid in a mixture of isopropanol and ethyl acetate. Other chiral acids (*N*-acetyl leucine, mandelic acid, and tartaric acid) showed poor performance as resolving agents. The (*S,S*)-salt of malic acid/**8** crystallized preferentially (6:94 diastereomeric ratio, d.r.) and a second

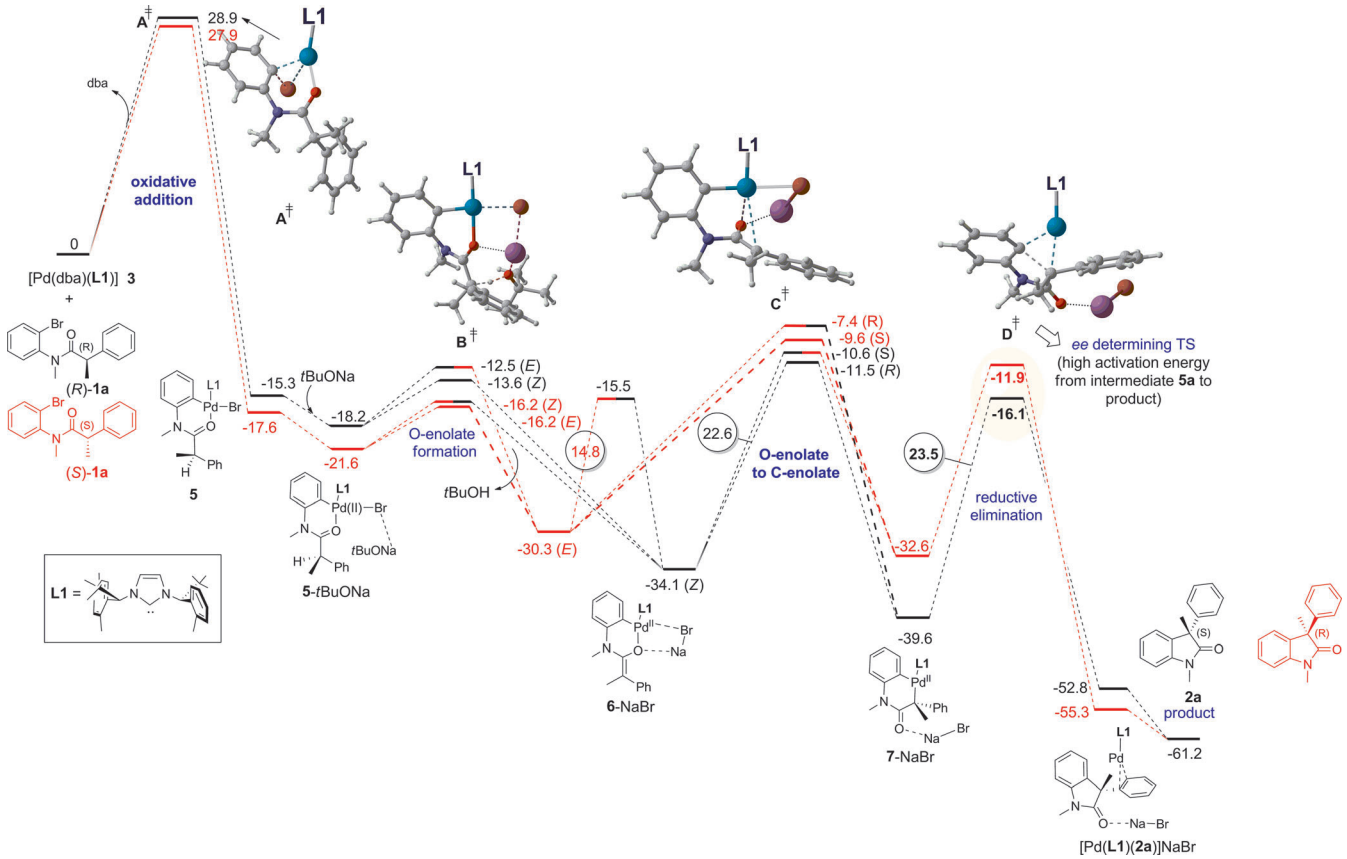

Figure 4. Gibbs free energy diagram (in kcal mol^{-1}) of key steps in the asymmetric synthesis of oxindole (*S*)-**2a** in solution at the SMD$_{1,4\text{-dioxane}}$/B3LYP/6-311+G** (C,H,N,O,Na,Br); LANL2TZ(f)(Pd)//B3LYP/6-31G*(C,H,N,O,Na,Br); LANL2DZ(Pd) level of theory. Transition-states **A**‡–**D**‡ and intermediates shown are those derived from the (*R*)-enantiomer of the starting material.

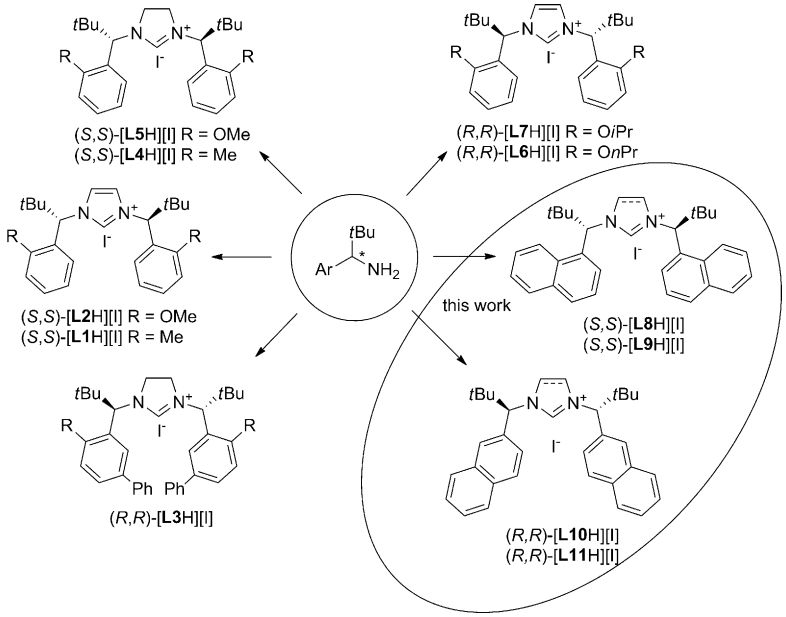

Scheme 4. Ligand library of chiral NHCs.

recrystallization furnished, after hydrolysis, the amine (*S*)-**8** in 38% overall yield (max.=50%) with >99% *ee*. For the resolution of amine **9** (L)-tartaric acid was found to give the best results. After two recrystallizations of the (*R,R*)-salt of tartaric acid/**9** in ethanol and amine recovery, (*R*)-**9** was obtained in 36% overall yield with 99% *ee*.

With the chiral amines in hand, the imidazolium salts [**L8**H][I]and [**L10**H][I] were synthesized by following literature methods.[15a,d–f] The chiral amines were condensed with glyoxal and the resulting diimines were reacted with chloromethylpivalate in the presence of silver triflate to obtain the imidazolium triflates. Anion exchange to the corresponding iodides gave solid products instead of oily triflate salts. Overall, this procedure is quite simple and no further purification of intermediates is needed. The product yields were modest.

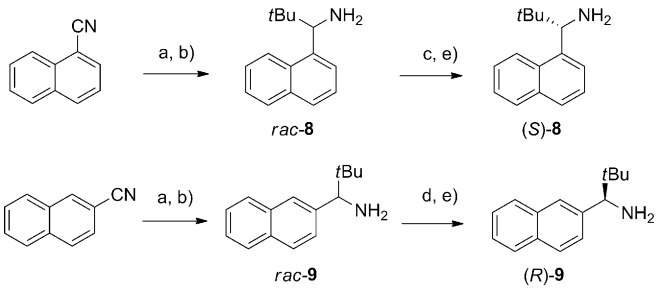

Scheme 5. Chiral amines (*S*)-**8** and (*R*)-**9** for the synthesis of imidazolium and dihydroimidazolium salts: a) *t*BuMgCl, CuBr (cat.), Et_2O, reflux 24 h; b) $NaBH_4$, MeOH, −78 to 25 °C, 16 h; c) (L)-maleic acid, *i*PrOH/EtOAc; d) (L)-(+)-tartaric acid, EtOH; e) 1 M NaOH, Et_2O.

For the synthesis of dihidroimidazolium salts [(*S*,*S*)-**L9**H][I] and [(*R*,*R*)-**L11**H][I], the diimines were reduced with $LiAlH_4$ to the corresponding diamines. Ring-closure was carried out according to the standard procedure with triethylorthoformate and NH_4BF_4. This afforded the tetrafluoroborate dihydroimidazolium salts. Anion exchange BF_4^-/I^- afforded dihydroimidazolium iodide salts in high yields (Scheme 6).

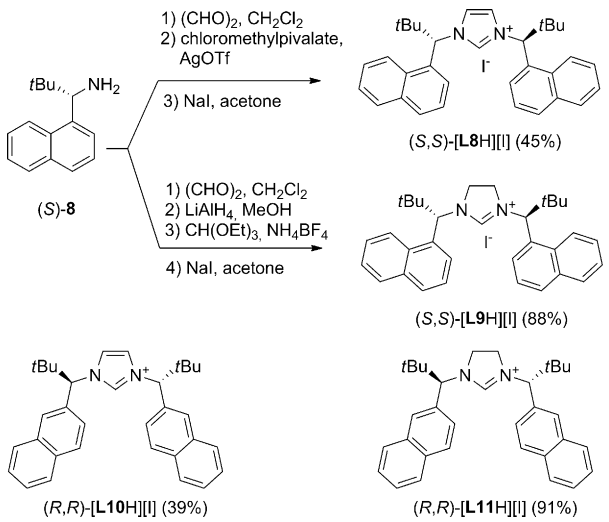

Scheme 6. Synthesis of imidazolium and dihydroimidazolium ligand precursors.

In extension of the modification of C_2-symmetric NHC ligands, the three C_1-symmetric imidazolium salts [**L12**H][BF_4]–[**L14**H][BF_4] were prepared by the route reported by the Fürstner group.[25] Nucleophilic addition of 2,6-diisopropylaniline to bromoacetaldehyde diethyl acetal in the presence of *n*BuLi led to the β-amino acetal **10** in excellent yield. The formamide derivative **11** was synthesized by treating **10** with HCO_2H in acetic anhydride and was obtained in near quantitative yield (Scheme 7).[26]

The acetoxyoxazolinium tetrafluoroborate derivative **12** was obtained as a white solid by treating **11** with $HBF_4 \cdot Et_2O$ in acetic anhydride. It was engaged in the next step by reaction with the requisite enantiopure amine. The hydroxylated

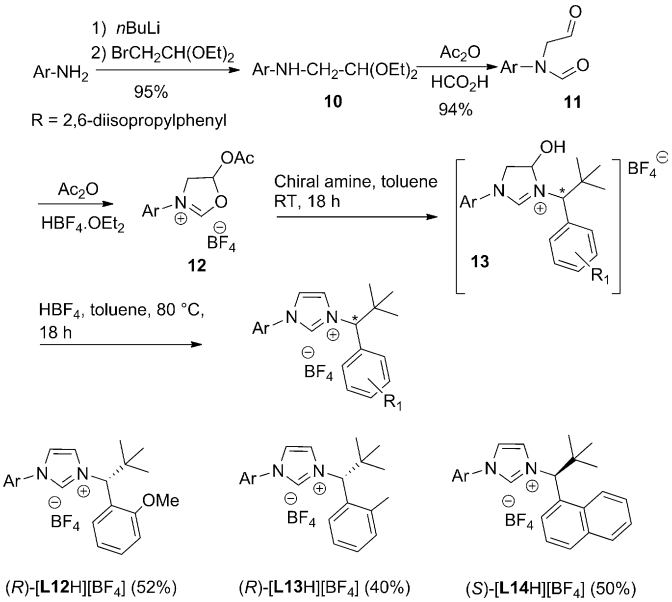

Scheme 7. Synthesis of C_1-symmetric imidazolium salts.

imidazolium salt **13** thus formed was treated with HBF_4 at 80 °C. The imidazolium salts [**L12**H][BF_4]–[**L14**H][BF_4] were isolated by flash column chromatography in moderate yield (40–52 %; over the last three steps).

Palladium-catalyzed synthesis of oxindoles: Catalysis with the new ligand (*S*,*S*)-[**L8**H][I] and, in less detail, with [**L12**H][BF_4]–[**L14**H][BF_4] was probed by applying previously reported methodology.[15d–f] As is immediately apparent from the data in Table 1, the ligands [**L12**H][BF_4]–[**L14**H][BF_4], while leading to fast reactions, fell far short in asymmetric induction (Table 1, entries 2–4). Conversely, (*S*,*S*)-[**L8**H][I] gave identical or slightly better yields than reactions with (*S*,*S*)-[**L1**H][I] or (*S*,*S*)-[**L2**H][I] and it outperformed these ligands in asymmetric induction by 2–3 % *ee*, a significant improvement in the 90–95 % *ee* range.

The optimized reaction conditions were applied to substrates leading to the spirocyclic products **15a**–**d** (Table 2) and **17a**–**n** (Table 3). A very important increase in asymmetric induction is observed for **15b** (Table 2, entry 3). This spiroxindole had been obtained previously in only 59 % *ee* (using **L1**).[15e] Yields were good to excellent throughout. Products were generally obtained with high asymmetric induction. Exceptions are **15a** incorporating a four-membered spirocyclic system and **17f** bearing an *o*-CF_3 group.

Table 3, entries 9–12, demonstrate that the reaction tolerates different N-protecting groups albeit that Bn, methoxymethyl ether (MOM), and benzyloxymethyl acetal (BOM) derivatives formed products with somewhat lower enantiomeric purity relative to *N*-Me due to the required heating to 50 °C with MOM and BOM protection (entries 11–12).[27]

3,3-Disubstituted aza-oxindoles form an important family of biologically active products.[28] A literature search revealed only a very limited number of reports for the synthesis of compounds containing the aza-oxindole motif.[29]

Table 1. Palladium-catalyzed α-arylation of **1a–d** by using (*S*,*S*)-**L8**, **L12**–**L14**.[a]

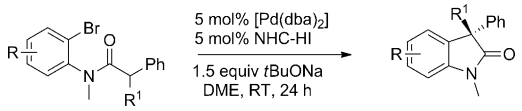

1 (*S*)-**2**

Entry	Product	Ligand precursor	Yield [%][b]	*ee* [%][c]
1	(*S*)-**2a**	(*S*,*S*)-[**L8**H][I]	99	96
2[d]		(*R*,*R*)-[**L12**H][BF_4]	95	−25
3[d]		(*R*)-[**L13**H][BF_4]	99	−18
4[d]		(*S*)-[**L14**H][BF_4]	98	0
5	(*S*)-**2b**	(*S*,*S*)-[**L8**H][I]	99	97
6	(*S*)-**2c**	(*S*,*S*)-[**L8**H][I]	97	96
7	(*S*)-**2d**	(*S*,*S*)-[**L8**H][I]	85	93

[a] 0.2 mmol substrate, 0.05 M in DME, absolute configurations of **2b–d** were assigned by comparison of the CD spectrum with that of (*S*)-**2a**.[15d,e] [b] Isolated yield. [c] The enantiomeric ratio was determined by HPLC analysis on a chiral stationary phase. [d] Reaction time is 3 h.

Table 2. Ring-size effect in asymmetric synthesis of spirooxindoles.[a]

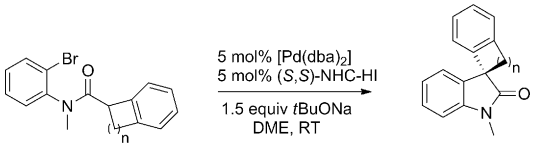

14a-d (*S*)-**15a-d**

Entry	Product	Ligand precursor	Yield [%][b]	*ee* [%][c]
1[d]	(S)-**15a**	(*S*,*S*)-[**L8**H][I]	89	23
2[d]		(*S*,*S*)-[**L2**H][I]	82	52
3[e]	(*S*)-**15b**	(*S*,*S*)-[**L8**H][I]	99	81
4[f]	(*S*)-**15c**	(*S*,*S*)-[**L8**H][I]	96	86
5[f]	(*S*)-**15d**	(*S*,*S*)-[**L8**H][I]	97	83

[a] 0.2 mmol substrate with 0.05 M in DME, absolute configurations were assigned by analogy and were tentative. [b] Isolated yield. [c] The enantiomeric ratio was determined by HPLC analysis on a chiral stationary phase. [d] 36 h. [e] 20 min. [f] 48 h.

Table 3. Palladium-catalyzed α-arylation of **16**.[a]

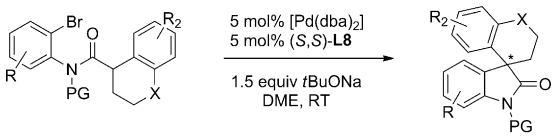

16 **17**

Entry	Product	*t* [min]	Yield [%][b]	*ee* [%][c]
1[d]	(*R*)-**17a**	10	98	−87
2[d]	(*R*)-**17b**	48	95	−89
3[d]	(*R*)-**17c**	10	89	−74
4	(*R*)-**17d**	10	77	−51
5[d]	(*R*)-**17e**	48	91	−77
6	(*S*)-**17f**	10	95	4
7	(*R*)-**17g**	48	92	88
8	(*R*)-**17i-l**	48	98	88
	(*S*)-**17j**			
9	PG = Me, (*R*)-**17i**	48	98	90
10	PG = Bn, (*R*)-**17j**	48	94	84
11[e]	PG = MOM, (*R*)-**17k**	24	97	86
12[e]	PG = BOM, (*R*)-**17l**	24	94	86
13	(*S*)-**17m**	48	75	56

[a] 0.2 mmol substrate with 0.05 M in DME, absolute configurations were assigned by analogy and were tentative. [b] Isolated yield. [c] Enantiomeric ratio was determined by HPLC analysis on a chiral stationary phase. [d] (*R*,*R*)-[**L8**H][I] was used. [e] 50 °C.

Table 4. Enantioselective synthesis of aza-spirooxindoles by palladium-catalyzed α-arylation.[a]

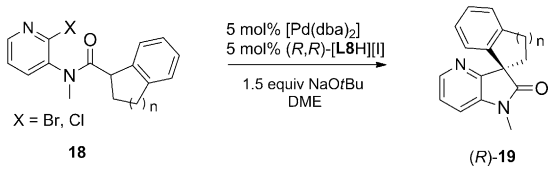

18 (*R*)-19

Entry	Product	*t* [h]/*T* [°C]	Yield [%][b]	ee [%][c]
1[d]	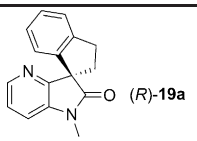 (*R*)-**19a**	0.2/25	99	84
2[d]		24/−10	99	86
3[d]	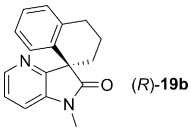 (*R*)-**19b**	0.3/25	99	88
4[d]		24/−10	99	91
5[e]		24/25	86	88
6[d]	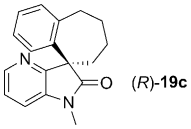 (*R*)-**19c**	0.3/25	99	86
7[d]		24/−10	99	90

[a] 0.2 mmol substrate with 0.05 M in DME, absolute configurations were assigned by analogy and were tentative. [b] Isolated yield. [c] Enantiomeric ratio was determined by chiral HPLC analyis. [d] X = Br. [e] X = Cl.

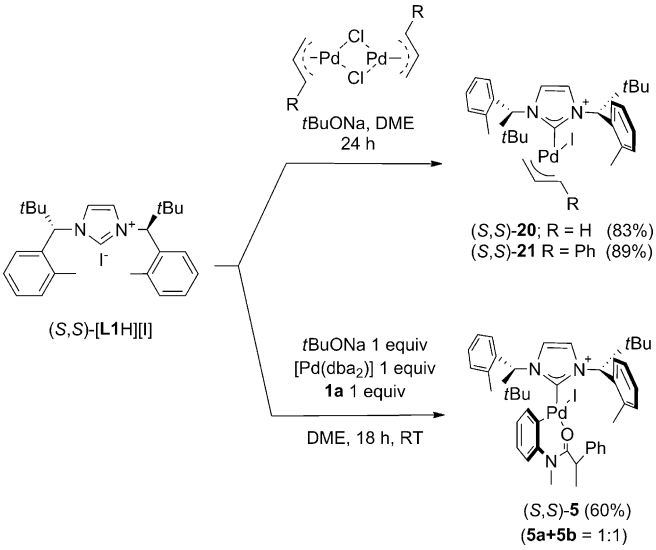

Scheme 8. Synthesis of chiral Pd–NHC complexes.

Enantioenriched aza-spiro-oxindoles are accessible using the arylation procedure as shown in Table 4. The short reaction times of *ortho*-pyridyl-based substrates is attributed to the faster oxidative addition of electron-poor aryl bromides to palladium.[30] Carrying out the reaction at −10 °C allowed us to improve the enantioselectivty of aza-spirooxindoles **19a–c** (Table 4, entries 2, 4, and 7). Finally, we were pleased to see that the pyridyl chloride substrate **18a** undergoes the cyclization reaction even at room temperature, producing, after 24 h, the desired product in 86 % yield with 88 % *ee* (entry 5).

Isolation of metallacycle intermediates and their application as catalysts: In all of our previous studies of oxindole and azaoxindole products, we used an in situ procedure to generate the chiral Pd^0–NHC* (NHC* = **L1**–**L11**) catalysts. Generation of [Pd^0(**L1**)] involved treating a mixture of [Pd_2(dba)$_2$] and the imidazolium iodide [(*S*,*S*)-**L1**H][I] in dimethoxyethane with *t*BuONa. An excess of base was used that then generated the amide enolate from the initially formed palladacycle **5** (Scheme 3).[14]

Complexes **20** and **21** were obtained readily by reaction of [Pd{(*R*)-allyl}Cl]$_2$ and [Pd{(*R*)-cinnamyl}Cl]$_2$, respectively, with imidazolium salt (*S*,*S*)-[**L1**H][I] and *t*BuONa. The reaction was carried out in DME at RT and produced the air and moisture-stable (*S*,*S*)-**20** and (*S*,*S*)-**21** in high yields (Scheme 8).

The reaction of exactly one equivalent of base together with aryl bromide **1a**, chiral imidazolium salt (*S*,*S*)-[**L1**H][I], and a stoichiometric amount of [Pd(dba)$_2$] in DME afforded complex **5** as a 1:1 mixture of diastereoisomers (**5a**/**5b**) in 60 % yield (Scheme 8).

Table 5 summarizes the results of the reaction depicted in Scheme 2. The catalytic activity of **5**, **20**, and **21** was compared to the original in situ procedure. The reaction using in situ generation of the catalyst was monitored by GC analysis. This showed complete conversion of starting material to oxindole **2a** in 4 h (Table 5, entry 1). Reactions carried out with (*S*,*S*)-**20** in the presence of *t*BuONa showed very poor conversion at RT (entry 2). Although subject to a nucleophilic addition/ligand exchange under milder conditions, the cinnamyl complex **21** behaved analogously (entry 3). Raising the temperature to 50 °C in this case led to the formation of oxindole **2a** in quantitative yield in 48 h with 90 % enantioselectivity (entry 4). The use of *t*BuOK was superior as shown in entries 5 and 6, but the reaction was still not as efficient as the in situ procedure.

Table 5. Intramolecular arylation of anilide **1a** (see Scheme 2) by using either in situ generated or preformed Pd^0–(*S*,*S*)-**L1** catalysts.[a]

Entry	Cat. (5 mol %)	Base (1.5 equiv)	*t* [h]	Yield [%][b]	*ee* [%][c]
1[d]	in situ	*t*BuONa	4	99	94
2	(*S*,*S*)-**20**	*t*BuONa	24	<10	94
3	(*S*,*S*)-**21**	*t*BuONa	24	<10	94
4[e]	(*S*,*S*)-**21**	*t*BuONa	48	99	90
5	(*S*,*S*)-**20**	*t*BuOK	24	98	94
6	(*S*,*S*)-**21**	*t*BuOK	24	98	94
7	(*S*,*S*)-**5**	*t*BuONa	24	65	94
8[f]	(*S*,*S*)-**5**	*t*BuONa	1.5	99	94

[a] 0.2 mmol substrate, 0.05 M in DME, 25 °C. [b] Isolated yield. [c] The enantiomeric ratio was determined by HPLC analysis on a chiral stationary phase. (Chiracel OD-H column). [d] 5 mol % (*S*,*S*)-[**L1**H][I], 5 mol % [Pd(dba)$_2$], 1.5 equiv *t*BuONa. [e] At 50 °C [f] Reaction performed with 10 mol % of dba.

Surprisingly, the palladacyle (*S*,*S*)-**5** was a poor performer as a catalyst. After 24 h, only 65% conversion of starting material was achieved (Table 5, entry 7). A clue here was the observation of some catalyst decomposition as indicated by the formation of palladium black. Adding dba restored catalyst lifetime and under these conditions the original in situ procedure could be improved (entry 8). The effect of other additives was probed (Figure 5). Not unexpectedly, P^{III}

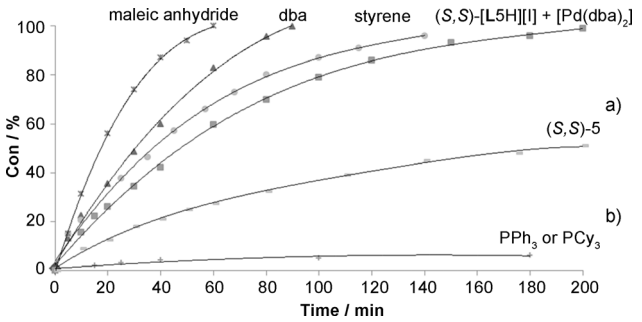

Figure 5. Effect of additives on the Pd-catalyzed α-arylation of amide **1a** to give **2a** by using a diasteromeric mixture of **5** as the catalyst. Reaction conditions: [**1a**] = 0.05 M, (*S*,*S*)-**5** 5 mol%, additive (10 mol%), *t*BuONa (1.5 equiv), DME, RT. Reaction monitored by GC analysis using decane as the internal standard. In all reactions, the oxindole **2a** formed in 94% *ee*. a) 65% conversion of starting material **1a** after 24 h. b) 7% conversion of starting material **1a** after 24 h.

ligands (PPh_3, PCy_3) interrupted the catalytic cycle, whereas alkenes rendered the process more efficient in the order of styrene < dba < maleic anhydride. In the presence of the alkenes (10 mol%), the half-life ($t_{1/2}$) of the first-order reaction was 39 (styrene), 30 (dba), and 19 min (maleic anhydride). This sequence likely reflects the ability of the alkenes to stabilize the Pd^0–NHC catalyst after a catalytic cycle. Electron-deficient olefins also decrease the activation energy barrier of the reductive elimination step.[31] Catalyst loading was reduced to 0.5 mol% with [**1a**] = 0.8 M, 1 mol% maleic anhydride (reaction time = 48 h). This produced 78% conversion of [**1a**] and a TON of 156. Asymmetric induction remained at 94% *ee* in all reactions.

Structure of metallacycles (*S*,*S*)-5a, (*S*,*S*)-5b, and (*S*,*S*)-22:[32] The diastereoisomers **5a** and **5b** were separated by column chromatography and were fully characterized. In (*S*,*S*)-**5b**, one of the *o*-methyl groups of the NHC ligand interacts with the aromatic system of the substrate. The ^1H NMR spectrum of (*S*,*S*)-**5b** shows a shift of close to $\delta =$ 1 ppm for these hydrogen atoms ((*S*,*S*)-**5a**, $\delta = 2.03$ ppm, (*S*,*S*)-**5b**, $\delta = 2.98$ ppm).

The palladacycles (*S*,*S*)-**22** and (*S*,*S*)-**23** were prepared analogously to **5** (Scheme 9) and the X-ray structure of (*S*,*S*)-**22** is included in Figure 5. Metallacycles (*S*,*S*)-**5a**, (*S*,*S*)-

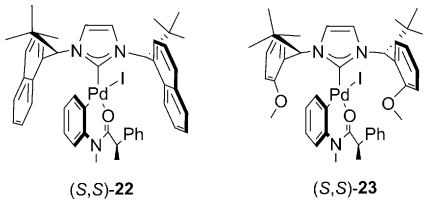

Scheme 9. Metallacycles incorporating ligands (*S*,*S*)-**L2** and (*S*,*S*)-**L8**. Synthesized according to the same procedure as shown in Scheme 4 ((*S*,*S*)-**22**, 64% yield; (*S*,*S*)-**23**, 58% yield).

5b, and (*S*,*S*)-**22** are slightly distorted square-planar [Pd^{II}-(NHC)] complexes with the iodide *trans* to the substrate aryl and the amide *trans* to the NHC ligand. The O-Pd-C_{NHC} angle in (*S*,*S*)-**5a** is 169.1°, and in (*S*,*S*)-**5b** it is 173.4°. Palladacycle (*S*,*S*)-**22** includes a π–π stacking arrangement between one of the naphthyl groups of the NHC ligand and the aryl group of the substrate (3.462 Å). This may be of some importance in the transition state leading to the product with high asymmetric induction. A comparison of the structures of the palladacycles show all stereoelements of the chiral ligand to be located similarly. The minimization of allylic strain ($A^{1,3}$), both in the Pd-C-*N*-C-H and also in H-$C_{benzylic}$-C_{Ar}-C_{ortho}-CH_3 parts of the ligand fix the aryl stereocontrol elements of the NHC ligand in the complex (Figure 6).

Overall, the ligand, when coordinated to Pd^{II} adopts an approximate C_2 chiral structure. In contrast, in the immidazolium salt both *t*Bu groups are in one hemisphere and the aryl groups are in the other with respect to the heterocycle plane.[15e,16]

Catalysis with palladacycles (*S*,*S*)-**22** and (*S*,*S*)-**23** (Scheme 9) in the presence of maleic anhydride proved slightly less efficient than with (*S*,*S*)-**5** (Figure 7).

Conclusion

The DFT computational analysis of the reaction mechanism reveals that the oxidative insertion of palladium–NHC* to C_{aryl}–Br bond initially generates a palladacycle, which upon deprotonation gives an O-enolate. The subsequent conversion of O-enolate to C-enolate followed by reductive elimination accounts for the asymmetric induction to give highly enantioenriched oxindoles. The metallacycles formed in the

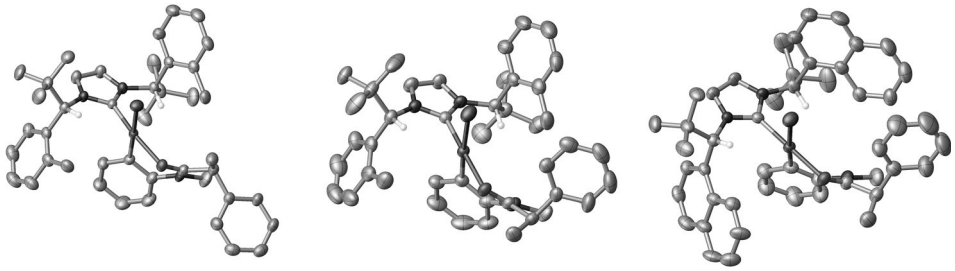

Figure 6. ORTEP diagrams of palladacycles left: (*S*,*S*)-**5a**, middle: (*S*,*S*)-**5b**, and right: (*S*,*S*)-**22** (50% probability level for the thermal ellipsoids). All H atoms except those on the stereogenic centers have been omitted for clarity.[31]

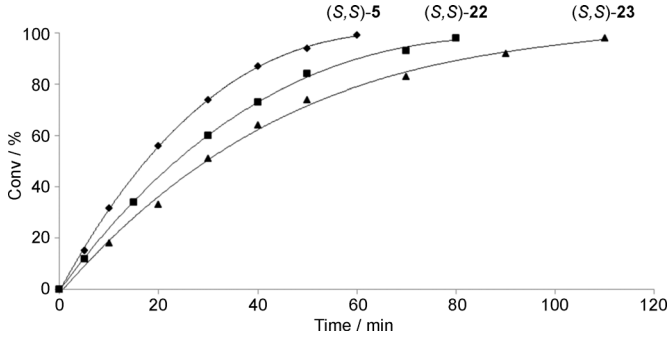

Figure 7. Variation of precatalysts in Pd-catalyzed α-arylation of amide **1a**. Reaction conditions: [**1a**] = 0.05 M, catalyst 5 mol%, maleic anhydride (10 mol%), *t*BuONa (1.5 equiv), DME, RT. Reaction was monitored by GC analysis using decane as the internal standard.

initial step were isolated and spectroscopically and structurally characterized. They are efficient catalysts for the reaction provided that an alkene is added to stabilize the Pd^0–NHC catalyst at the end of the catalytic cycle. New bulky NHC ligands were synthesized and one of them (**L8**) proved to vastly outperform previous catalysts in the reactions yielding spirooxindoles and aza-spirooxindoles.

Experimental Section

General: Solvents were purified by filtration on drying columns using a Solvtek system or by distillation over Na/benzophenone. Reactions and manipulations involving organometallic or moisture sensitive compounds were carried out under purified nitrogen in glassware dried by heating under high vacuum. M.p.: Büchi 510 (uncorrected). GC: Hewlett Packard 6890 gas chromatograph with FID detection using a Permabond OV-1701–0.25 column (25 m × 0.32 mm ID). HPLC: Agilent 1100 series chromatograph. NMR: Bruker AMX-500, AMX-400, or AMX-300 FT; internal D-lock. IR spectra: Perkin–Elmer Spectrum One. Neat liquids; Golden Gate accessory. HRMS: +TOF mode, ESI-MS mode, Applied Biosystems/Scix (Q-STA) spectrometer. $[\alpha]_D$: Perkin–Elmer 241 polarimeter, quartz cell (l = 10 cm), Na high-pressure lamp (λ = 589 nm). CD spectra: Jasco J-715, quartz cell (l = 1 cm).

Synthesis of *rac*-amine 8: A 250 mL flask, equipped with condenser and stirring bar was dried under vacuum by using a heat gun. After cooling under a current of N_2, it was charged with 1-naphonitrile (10.0 g, 65.35 mmol, 1.0 equiv), followed by *t*BuMgCl (40.35 mL of 1.7 M solution in Et_2O, 68.61 mmol, 1.05 equiv) and CuBr (262 mg, 2.8 mol%, 1.83 mmol). The reaction was refluxed for 24 h under N_2. After cooling to −78 °C, dry methanol (50 mL) was added cautiously followed by $NaBH_4$ (3.2 g, 85 mmol, 1.3 equiv) in two portions and the reaction was allowed to warm to RT over 6 h and stirred overnight. H_2O (50 mL) was added slowly and the precipitate was removed by filtration and washed with Et_2O. The filtrate was evaporated and the product was distilled under reduced pressure. The material obtained was dissolved in Et_2O and precipitated by adding 1 M HCl in Et_2O. The solid was suspended in Et_2O and then aq. NaOH (1 M) solution was added until a clear two-phase solution was obtained. The organic layer was separated and the aq. phase was washed repeatedly with small quantities of Et_2O. The combined organic phases were dried over $MgSO_4$. Filtration over Celite and evaporation of volatiles under reduced pressure afforded amine **8** as a colorless solid (9.30 g, 67%).

*2,2-Dimethyl-1-(naphthalen-1-yl)propan-1-amine (*rac-***8***)*: ^{1}H NMR (400 MHz, $CDCl_3$): δ = 1.02 (s, 9H), 1.59 (br s, 2H), 4.84 (s, 1H), 7.47–7.57 (m, 3H), 7.73–7.79 (m, 2H), 7.82 (d, J = 21 Hz, 1H), 8.26 ppm (d, J = 7.8 Hz, 1H); ^{13}C NMR (75 MHz, $CDCl_3$): δ = 26.9, 36.3, 57.2, 99.9, 123.8, 125.0, 125.10, 125.19, 125.4, 127.2, 128.9, 132.4, 133.5, 140.5 ppm; IR (neat, cm^{-1}): $\tilde{\nu}$ = 3366, 3296, 2962, 1948, 1594, 1509, 1473, 1389, 1358, 1328, 1069, 1026, 909, 872, 802, 780, 749, 633 cm^{-1}.

Resolution of amine *rac*-8: An equimolar mixture of *rac*-**8** (34.0 g, 159.62 mmol) and (L)-malic acid (21.4 g, 159.62 mmol) was placed in a 2 L round-bottomed flask equipped with a reflux condenser. *i*PrOH (900 mL) and EtOAc (120 mL) were added and the magnetically stirred mixture was heated to reflux until all the solid had dissolved. The flask was then placed in a cold room (5 °C) overnight. The crystalline precipitate was filtered from the mother liquid and washed with *i*PrOH (100 mL). After drying under vacuum, the enantiomerically enriched salt of amine **8** (23.2 g, 67.04 mmol, 42% yield) was obtained with 88% *ee* (checked by HPLC analysis after treating a sample with NaOH (1 N) and extracted with Et_2O: Chiracel OD-H column, *n*-hexane/*i*PrOH = 99:1, 1.0 mL min^{-1}, 254 nm; t_R = 26.09 (major) and 21.47 min (minor)). A second recrystallization was carried out by refluxing the salt of amine **8** (23.2 g, 67.04 mmol, 88% *ee*) in *i*PrOH (500 mL) and EtOAc (100 mL) until the solid had dissolved. The hot solution was cooled to RT overnight, crystals separated by filtration, washed with *i*PrOH (80 mL), and dried under vacuum. Addition of NaOH (1 N) and extraction with ether afforded amine (*S*)-**8** (12.90 g, 38%, >99% *ee*) as a colorless crystalline solid. M.p. 82–83 °C; $[\alpha]_D^{25}$ = −59.1 (c = 1.0 in CH_2Cl_2).

Representative procedure for the synthesis of imidazolium iodide salt (*S,S*)-[L8H][I]: Aq. glyoxal (40%; 690 μL, 6 mmol, 0.5 equiv) was introduced into dichloromethane (25 mL) and vigorously stirred with freshly dehydrated sodium sulfate (6.0 g). Formic acid (98%; 34 μL, 0.9 mmol, 7 mol%) and (*S*)-**8** (2.55 g, 12 mmol, 1.0 equiv) were added. The mixture was stirred for 5 min and then additional sodium sulfate (6.0 g) was added. During 5 h of stirring at RT the solution turned slightly yellow. The mixture was then filtered and the solvent was removed in vacuo to yield the diimine intermediate, which was purified by crystallization from MeOH.

Chloromethyl pivalate (0.47 mL, 3.26 mmol) was added to AgOTf (830 mg, 3.26 mmol) in CH_2Cl_2 (16 mL) and the resulting mixture was stirred for 45 min under N_2 in the absence of light. The resulting suspension was transferred via a cannula, equipped with a filter, into a second Schlenk tube containing the diimine (890 mg, 2.17 mmol). The solution was stirred in the absence of light at 40 °C for 24 h. The reaction was cooled to ambient temperature and the solvent was evaporated and subsequently taken up in dry acetone (10.0 mL). NaI (109 mg) was added and the reaction was stirred overnight. All volatiles were removed by evaporation. The residue was taken up in a small amount of $CHCl_3$ and filtered through cotton. The entire procedure for the ion exchange was repeated with NaI (99 mg, 1.0 equiv). Column chromatography (CH_2Cl_2/Et_2O 1:1) afforded the product (*S,S*)-[**L8**H][I] (574 mg, 45% yield over two steps). Yellow solid; m.p. 156–158 °C; $[\alpha]_D^{25}$ = +35.1 (c = 1.0 in CH_2Cl_2); ^{1}H NMR (400 MHz, $CDCl_3$): δ = 1.18 (s, 18H), 6.75 (s, 2H), 7.42 (d, J = 7.3 Hz, 2H), 7.49 (d, J = 1.5 Hz, 2H), 7.52 (t, J = 7.8 Hz, 2H), 7.61 (dd, J = 6.9, 1.3 Hz, 1H), 7.63 (dd, J = 6.9, 1.3 Hz, 1H), 7.80 (dd, J = 8.2, 0.6 Hz, 2H), 7.83 (d, J = 8.2 Hz, 2H), 8.04 (d, J = 6.7 Hz, 2H), 8.79 (d, J = 8.7 Hz, 2H), 11.48 ppm (s, 1H); ^{13}C NMR (100 MHz, $CDCl_3$): δ = 28.1, 37.3, 67.0, 122.0, 123.9, 124.9, 126.5, 126.6, 128.1, 129.2, 130.2, 131.0, 132.1, 134.2, 138.3 ppm; IR (neat, cm^{-1}): $\tilde{\nu}$ = 2962, 1599, 1536, 1476, 1369, 1140, 1030, 786, 756, 667 cm^{-1}; HRMS (EI): m/z: calcd for $C_{33}H_{37}N_2$: 461.2956 $[M-I]^+$; found: 461.2970.

Catalytic asymmetric intramolecular α-arylation reaction

Spirocyclic oxindole (*S*)-**15c**: Under N_2, a dried Schlenk tube was charged with $[Pd(dba)_2]$ (5.7 mg, 0.01 mmol), (*S,S*)-[**L8**H][I] (5.88 mg, 0.01 mmol), and *t*BuONa (28.8 mg, 0.3 mmol). Dimethoxyethane (DME) (1 mL) was added and the mixture was stirred for 10 min. Substrate **14c** (68.8 mg, 0.2 mmol) was then added as a solution in DME (3 mL). The reaction was stirred at RT for 48 h and then quenched with aq. NH_4Cl and extracted with diethyl ether. The combined organic phases were washed with water and brine and then dried over Na_2SO_4. Flash chromatography over SiO_2 afforded (*S*)-**15c** as a white solid (50.5 mg, 96%). M.p. 146–148 °C; $[\alpha]_D^{25}$ = +4.31 (c = 1.0 in CH_2Cl_2); 86% *ee* (Chiracel AS-H column, *n*-hexane/*i*PrOH = 98:2, 1.0 mL min^{-1}, 254 nm; t_R = 11.26 (major) and 15.46 min. (minor)); ^{1}H NMR (400 MHz, $CDCl_3$): δ = 1.98–

2.13 (m, 2H), 2.21–2.28 (m, 1H), 2.37–2.46 (m, 1H), 2.98–3.12 (m, 1H), 3.35 (s, 3H), 6.53 (d, J=7.7 Hz, 1H), 6.98 (d, J=7.8 Hz, 1H), 7.01 (t, J=8.0 Hz, 1H), 7.07 (d, J=8.0 Hz, 1H), 7.14 (d, J=8.0 Hz, 1H), 7.18 (t, J=8.0 Hz, 1H), 7.21 (d, J=8.0 Hz, 1H), 7.37 ppm (td, J=8.0, 1.3 Hz, 1H); ^{13}C NMR (75 MHz, $CDCl_3$): δ=18.7, 26.5, 29.7, 34.0, 52.2, 108.0, 122.8, 124.0, 126.3, 127.1, 127.8, 128.0, 129.7, 135.1, 137.3, 137.8, 143.1, 180.5 ppm; IR (neat, cm^{-1}): $\tilde{\nu}$=2933, 1707, 1610, 1491, 1342, 1255, 1125, 1091, 965, 749, 692 cm^{-1}; HRMS (EI): m/z: calcd for $C_{18}H_{17}NO$: 264.1382 $[M+H]^+$; found: 264.1388.

Computational methods: All calculations were carried out using the Gaussian 09 suite of quantum chemical programs.[33] The hybrid density-functional B3LYP was used for the calculations.[34] The LANL2DZ basis set consisting of effective core potential (ECP) for 28 electrons and Hay–Wadt's valance basis functions for all other electrons has been used for palladium and iodine.[35] The remaining elements (C,H,N,O,Br,Na) were represented by using the 6-31G* basis set.[36] In all computations, pure d functions were employed. The effect of solvent for the most preferred pathway was taken into account by computing the energy at the $SMD_{1,4\text{-dioxane}}$/B3LYP/6-311+G** (C,H,N,O,Br,Na); LANL2TZ(f)(Pd)// B3LYP/6-31G* (C,H,N,O,Br,Na); LANL2DZ(Pd) level of theory. The thermal and entropic corrections, as obtained at the B3LYP/6-31G*(C,H,N,O,Br,Na); LANL2DZ(Pd) level of theory, were included to the single-point energies obtained in the solvent continuum to estimate the Gibbs free energies. The closely related 1,4-dioxane was used as the solvent due to the lack of parameters for DME in the Gaussian 09 suite of programs. The nature of the stationary points was verified by the visual inspection of the imaginary frequencies pertaining to the desired reaction coordinate. The transition states were characterized by one and only one imaginary frequency representing the reaction coordinate. Further, the intrinsic reaction coordinate (IRC) calculations were performed to authenticate the transition states.[37] The final geometries obtained by IRC calculation were further subjected to optimization with "OPT=RCFC" option to obtain minima on either sides of the transition state. The discussion in the main text is based on the solvent phase energies. The gas phase energies are provided in the Supporting Information.

Acknowledgements

We thank the Swiss National Science Foundation (grant no. 200020 134682/1 to E.P.K.), BRNS-Mumbai (RBS), and the University of Geneva for financial support and the IITB computer center for computing time. A.K.S. acknowledges CSIR (New Delhi) for a senior research fellowship.

[1] a) J. F. M. da Silva, S. J. Garden, A. C. Pinto, *J. Braz. Chem. Soc.* **2001**, *12*, 273–324; b) B. S. Jensen, *CNS Drug Rev.* **2006**, *8*, 353–360; c) H. Lin, S. J. Danishefsky, *Angew. Chem.* **2003**, *115*, 38–53; *Angew. Chem. Int. Ed.* **2003**, *42*, 36–51; d) C. Marti, E. M. Carreira, *Eur. J. Org. Chem.* **2003**, 2209–2219; e) C. V. Galliford, K. A. Scheidt, *Angew. Chem.* **2007**, *119*, 8902–8912; *Angew. Chem. Int. Ed.* **2007**, *46*, 8748–8758; f) A. Fensome, W. R. Adams, A. L. Adams, T. J. Berrodin, J. Cohen, C. Huselton, A. Illenberger, J. C. Kern, V. A. Hudak, M. A. Marella, E. G. Melenski, C. C. McComas, C. A. Mugford, O. D. Slayden, M. Yudt, Z. M. Zhang, P. W. Zhang, Y. Zhu, R. C. Winneker, J. E. Wrobel, *J. Med. Chem.* **2008**, *51*, 1861–1873.

[2] a) B. Trost, M. K. Brennan, *Synthesis* **2009**, 3003–3025; b) F. Zhou, Y.-L. Liu, J. Zhou, *Adv. Synth. Catal.* **2010**, *352*, 1381–1407; c) J. E. M. N. Klein, R. J. K. Taylor, *Eur. J. Org. Chem.* **2011**, 6821–6841.

[3] Enantioselective nucleophilic addition to isatins: a) G. Luppi, P. G. Cozzi, M. Monari, B. Kaptein, Q. B. Broxterman, C. Tomasini, *J. Org. Chem.* **2005**, *70*, 7418–7421; b) R. Shintani, M. Inoue, T. Hayaashi, *Angew. Chem.* **2006**, *118*, 3431–3434; *Angew. Chem. Int. Ed.* **2006**, *45*, 3353–3356; c) P. Y. Toullec, R. B. C. Jagt, J. G. de Vries, B. L. Feringa, A. J. Minnaard, *Org. Lett.* **2006**, *8*, 2715–2718; d) G. Luppi, M. Monari, R. J. Corrêa, F. A. Violante, A. C. Pinto, B. Kaptein, Q. B. Broxterman, S. J. Garden, C. Tomasini, *Tetrahedron* **2006**, *62*, 12017–12024; e) M. Kitajima, I. Mori, K. Arai, N. Kogure, H. Takayama, *Tetrahedron Lett.* **2006**, *47*, 3199–3202; f) J.-R. Chen, X.-P. Liu, X.-Y. Zhu, L. Li, Y.-F. Qiao, J.-M. Zhang, W.-J. Xiao, *Tetrahedron* **2007**, *63*, 10437–10444; g) S. Nakamura, N. Hara, H. Nakashima, K. Kubo, N. Shibata, T. Toru, *Chem. Eur. J.* **2008**, *14*, 8079–8081; h) B. Alcaide, P. Almendros, *Angew. Chem.* **2008**, *120*, 4710–4712; *Angew. Chem. Int. Ed.* **2008**, *47*, 4632–4634; i) X. Cheng, S. Vellalath, R. Goddard, B. List, *J. Am. Chem. Soc.* **2008**, *130*, 15786–15787; j) T. Itoh, H. Ishikawa, Y. Hayashi, *Org. Lett.* **2009**, *11*, 3854–3857; k) F. Xue, S. Zhang, L. Liu, W. Duan, W. Wang, *Chem. Asian J.* **2009**, *4*, 1664–1667; l) D. Tomita, K. Yamatsugu, M. Kanai, M. Shibasaki, *J. Am. Chem. Soc.* **2009**, *131*, 6946–6948; m) J. Itoh, S. B. Han, M. J. Krische, *Angew. Chem.* **2009**, *121*, 6431–6434; *Angew. Chem. Int. Ed.* **2009**, *48*, 6313–6316; n) V. Hanhan, A. H. Sahin, T. W. Chang, J. C. Fettinger, A. K. Franz, *Angew. Chem.* **2010**, *122*, 756–759; *Angew. Chem. Int. Ed.* **2010**, *49*, 744–747; o) J. Deng, S. Zhang, P. Ding, H. Jiang, W. Wang, J. Li, *Adv. Synth. Catal.* **2010**, *352*, 833–838.

[4] Oxindole synthesis by alkylation reaction: a) T. B. K. Lee, G. S. K. Wong, *J. Org. Chem.* **1991**, *56*, 872–875; b) B. M. Trost, M. U. Frederiksen, *Angew. Chem.* **2005**, *117*, 312–314; *Angew. Chem. Int. Ed.* **2005**, *44*, 308–310; c) B. M. Trost, Y. Zhang, *J. Am. Chem. Soc.* **2006**, *128*, 4590–4591; d) B. M. Trost, Y. J. Zhang, *J. Am. Chem. Soc.* **2007**, *129*, 14548–14549; e) B. M. Trost, Y. Zhang, *Chem. Eur. J.* **2010**, *16*, 296–303; f) K. Jiang, J. Peng, H.-L. Cui, Y.-C. Chen, *Chem. Commun.* **2009**, 3955–3957; g) Z.-K. Xiao, H.-Y. Yin, L.-X. Shao, *Org. Lett.* **2013**, *15*, 1254–1257.

[5] Oxindole synthesis by fluorination reaction: a) Y. Hamashima, T. Suzuki, H. Takano, Y. Shimura, M. Sodeoka, *J. Am. Chem. Soc.* **2005**, *127*, 10164–10165; b) N. Shibata, J. Kohno, K. Takai, T. Ishimaru, S. Nakamura, T. Toru, S. Kanemasa, *Angew. Chem.* **2005**, *117*, 4276–4279; *Angew. Chem. Int. Ed.* **2005**, *44*, 4204–4207; c) T. Ishimaru, N. Shibata, T. Horikawa, N. Yasuda, S. Nakamura, T. Toru, M. Shiro, *Angew. Chem.* **2008**, *120*, 4225–4229; *Angew. Chem. Int. Ed.* **2008**, *47*, 4157–4161.

[6] Oxindole synthesis by hydroxylation reaction: a) T. Ishimaru, N. Shibata, J. Nagai, S. Nakamura, T. Toru, S. Kanemasa, *J. Am. Chem. Soc.* **2006**, *128*, 16488–16489; b) D. Sano, K. Nagata, T. Itoh, *Org. Lett.* **2008**, *10*, 1593–1595.

[7] Oxindole synthesis by aldol reaction: a) ref. [6b]; b) S. Ogawa, N. Shibata, J. Inagaki, S. Nakamura, T. Toru, M. Shiro, *Angew. Chem.* **2007**, *119*, 8820–8823; *Angew. Chem. Int. Ed.* **2007**, *46*, 8666–8669; c) S. Kobayashi, M. Kokubo, K. Kawasumi, T. Nagano, *Chem. Asian J.* **2010**, *5*, 490–492; d) K. Shen, X. Liu, K. Zheng, W. Li, X. Hu, L. Lin, X. Feng, *Chem. Eur. J.* **2010**, *16*, 3736–3742.

[8] Oxindole synthesis by Mannich reaction: a) X. Tian, K. Jiang, J. Peng, W. Du, Y.-C. Chen, *Org.Lett.* **2008**, *10*, 3583–3586; b) L. Cheng, L. Liu, H. Jia, D. Wang, Y.-J. Chen, *J. Org. Chem.* **2009**, *74*, 4650–4653; c) R. He, C. Ding, K. Maruoka, *Angew. Chem.* **2009**, *121*, 4629–4631; *Angew. Chem. Int. Ed.* **2009**, *48*, 4559–4561.

[9] Oxindole synthesis by Michael addition reaction: a) P. Galzerano, G. Bencivenni, F. Pesciaioli, A. Mazzanti, B. Giannichi, L. Sambri, G. Bartoli, P. Melchiorre, *Chem. Eur. J.* **2009**, *15*, 7846–7849; b) X. Li, Z.-G. Xi, S. Luo, J.-P. Cheng, *Org. Biomol. Chem.* **2010**, *8*, 77–82; c) T. Bui, S. Syed, C. F. Barbas III, *J. Am. Chem. Soc.* **2009**, *131*, 8758–8759; d) Y. Kato, M. Furutachi, Z. Chen, H. Mitsunuma, S. Matsunaga, M. Shibasaki, *J. Am. Chem. Soc.* **2009**, *131*, 9168–9169; e) R. He, S. Shirakawa, K. Maruoka, *J. Am. Chem. Soc.* **2009**, *131*, 16620–16621; f) X. Li, B. Zhang, Z.-G. Xi, S. Luo, J.-P. Cheng, *Adv. Synth. Catal.* **2010**, *352*, 416–424.

[10] Oxindole synthesis by amination reaction: a) L. Cheng, L. Liu, D. Wang, Y.-J. Chen, *Org. Lett.* **2009**, *11*, 3874–3877; b) Z.-Q. Qian, F. Zhou, T.-P. Du, B.-L. Wang, M. Ding, X.-L. Zhao, J. Zhou, *Chem. Commun.* **2009**, 6753–6755; c) T. Bui, M. Borregan, C. F. Barbas II, *J. Org. Chem.* **2009**, *74*, 8935–8938; d) S. Mouri, Z. Chen, H. Mitsunuma, M. Furutachi, S. Matsunaga, M. Shibasaki, *J. Am. Chem. Soc.* **2010**, *132*, 1255–1257.

[11] Oxindole synthesis by arylation reaction: A. M. Taylor, R. A. Altman, S. L. Buchwald, *J. Am. Chem. Soc.* **2009**, *131*, 9900–9901.
[12] a) N. E. Carpenter, D. J. Kucera, L. E. Overman, *J. Org. Chem.* **1989**, *54*, 5846–5848; b) L. E. Overman, D. J. Poon, *Angew. Chem.* **1997**, *109*, 536–538; *Angew. Chem. Int. Ed. Engl.* **1997**, *36*, 518–521; c) A. Ashimori, B. Bachand, M. A. Calter, S. P. Govek, L. E. Overman, D. J. Poon, *J. Am. Chem. Soc.* **1998**, *120*, 6488–6499; d) A. Ashimori, B. Bachand, L. E. Overman, D. J. Poon, *J. Am. Chem. Soc.* **1998**, *120*, 6477–6487.
[13] A. Pinto, Y. Jia, L. Neuville, J. Zhu, *Chem. Eur. J.* **2007**, *13*, 961–967.
[14] S. Lee, J. F. Harwig, *J. Org. Chem.* **2001**, *66*, 3402–3415.
[15] a) F. Glorius, G. Altenhoff, R. Goddard, C. Lehmann, *Chem. Commun.* **2002**, 2704–2705; b) T. Arao, K. Kondo, T. Aoyama, *Tetrahedron Lett.* **2006**, *47*, 1417–1420; c) T. Arao, K. Sato, K. Kondo, T. Aoyama, *Chem. Pharm. Bull.* **2006**, *54*, 1576–1581; d) E. P. Kündig, T. M. Seidel, Y.-X. Jia, G. Bernardinelli, *Angew. Chem.* **2007**, *119*, 8636–8639; *Angew. Chem. Int. Ed.* **2007**, *46*, 8484–8487; e) Y.-X. Jia, D. Katayev, G. Bernardinelli, T. M. Seidel, E. P. Kündig, *Chem. Eur. J.* **2010**, *16*, 6300–6309; f) Y.-X. Jia, J. M. Hillgren, E. L. Watson, S. P. Marsden, E. P. Kündig, *Chem. Commun.* **2008**, 4040–4042; g) D. Katayev, E. P. Kündig, *Helv. Chim. Acta.* **2012**, *95*, 2287–2295; h) X. Luan, R. Mariz, C. Robert, M. Gatti, S. Blumentritt, A. Linden, R. Dorta, *Org. Lett.* **2008**, *10*, 5569–5572; i) X. J. Luan, L. L. Wu, E. Drinkel, R. Mariz, M. Gatti, R. Dorta, *Org. Lett.* **2010**, *12*, 1912–1915; j) L. Wu, L. Falivene, E. Drinkel, S. Grant, A. Linden, L. Cavallo, R. Dorta, *Angew. Chem.* **2012**, *124*, 2924–2927; *Angew. Chem. Int. Ed.* **2012**, *51*, 2870–2873; k) S. Wurtz, C. Lohre, R. Frohlich, K. Bergander, F. Glorius, *J. Am. Chem. Soc.* **2009**, *131*, 8344–8345; l) L. T. Liu, N. Ishida, S. Ashida, M. Murakami, *Org. Lett.* **2011**, *13*, 1666–1669; m) M. J. Spallek, D. Riedel, F. Rominger, A. S. K. Hashmi, O. Trapp, *Organometallics* **2012**, *31*, 1127–1132.
[16] a) D. Banerjee, C. Besnard, E. P. Kündig, *Organometallics* **2012**, *31*, 709–715; b) D. Banerjee, A. Buzas, C. Besnard, E. P. Kündig, *Organometallics* **2012**, *31*, 8348–8354; c) E. Larionov, M. Nakanishi, D. Katayev, E. P. Kündig, *Chem. Sci.* **2013**, *4*, 1995–2005.
[17] a) M. Nakanishi, D. Katayev, C. Besnard, E. P. Kündig, *Angew. Chem.* **2011**, *123*, 7576–7579; *Angew. Chem. Int. Ed.* **2011**, *50*, 7438–7441; b) D. Katayev, M. Nakanishi, T. Bürgi, E. P. Kündig, *Chem. Sci.* **2012**, *3*, 1422–1425.
[18] J. Mandel, X. Pan, E. B. Hay, S. J. Geib, C. S. Wilcox, D. P. Curran, *J. Org. Chem.* **2013**, *78*, 4083–4089.
[19] NaBr either remains with the system until the product is formed or is expelled from the enolate. Another situation in which only *t*BuO$^-$ facilitates the deprotonation, in the absence of sodium ion, is also examined. More details (pathways **A1**–**A5**) can be found in the Supporting Information (p. S116).
[20] a) Another geometric analogue TS**A′** was also identified. It leads to a similar tetracoordinate intermediate **5′**, in which C_{aryl}–Br and NHC are *anti* to each other. This is higher in energy than **5**. b) The optimized geometries of other transition states for formation of **5** are provided in Figure S1 in the Supporting Information.
[21] Optimized geometries for the deprotonation are provided in Figure S5 in the Supporting Information.
[22] The optimized geometries of two other transition states involved in the conversion of O-enolate to C-enolate are provided in Figure S6 in the Supporting Information. Alternatively, a higher energy pathway consisting of a different isomer **27′** (**27**+NaBr), in which NaBr is bound to the enolate oxygen atom was also examined (see Scheme S2 and Figure S7 in the Supporting Information). Rotation around the C–N bond in **27′** can directly furnish the C-enolate **7**.
[23] Another possibility involves C–C bond formation when Br is in the coordination sphere of Pd maintaining an interaction with Na. The energy barrier for the C–C bond formation TS in this mode is found to be higher. The geometries for this possibility are provided in Figure S10, TS-(**7*R*-2*S***)$_{Conf^-PdBr}$, in the Supporting Information.
[24] See the Supporting Information for 1) a complete mapping of the atomic contacts that supports the distortion (Figure S14–S15) and 2) details of activation strain analysis (Table S2).
[25] A similar geometric feature is noted in the X-ray crystal structure of intermediate **5** in which the substrate stays closer towards the *tert*-butyl group of the catalyst.
[26] A. Fürstner, M. Alcarazo, V. Cesar, C. W. Lehmann, *Chem. Commun.* **2006**, 2176–2178.
[27] For an application of the BOM and MOM protecting groups in an asymmetric synthesis application of an oxindole product, see: D. Katayev, E. P. Kündig, *Helv. Chim. Acta* **2012**, *95*, 2287–2295.
[28] a) C. P. Ting, J. J. Kaminski, M. H. Sherlock, W. C. Tom, J. F. Lee, R. W. Bryant, A. S. Watnick, A. T. McPhail, *J. Med. Chem.* **1990**, *33*, 2697–2706; b) V. Kumar, J. A. Dority, E. R. Bacon, B. Singh, G. Y. Lesher, *J. Org. Chem.* **1992**, *57*, 6995–6998; c) M. Cheung, R. N. Hunter III, M. R. Peel, K. E. Lackey, *Heterocycles* **2001**, *55*, 1583–1590; d) C. Adams, D. J. Aldous, S. Amendola, P. Bamborough, C. Bright, S. Crowe, P. Eastwood, G. Fenton, M. Foster, T. K. P. Harrison, S. King, J. Lai, C. Lawrence, J. P. Letallec, C. McCarthy, N. Moorcroft, K. Page, S. Rao, J. Redford, S. Sadiq, K. Smith, J. E. Souness, S. Thurairatnam, M. Vine, B. Wyman, *Bioorg. Med. Chem. Lett.* **2003**, *13*, 3105–3110; e) E. R. Wood, L. Kuyper, K. G. Petrov, R. N. Hunter III, P. A. Harris, K. Lackey, *Bioorg. Med. Chem. Lett.* **2004**, *14*, 953–957.
[29] a) F. Johnson, S. K. Malhorta, *J. Am. Chem. Soc.* **1965**, *87*, 5492–5493; For reviews, see b) R. W. Hoffmann, *Chem. Rev.* **1989**, *89*, 1841–1860; c) R. W. Hoffmann, *Angew. Chem.* **2000**, *112*, 2134–2150; *Angew. Chem. Int. Ed.* **2000**, *39*, 2054–2070; d) E. V. Anslyn, D. A. Dougherty, *Modern Physical Organic Chemistry*, University Science Books, **2006**.
[30] M. Lemhardi, Y. Fall, H. Doucet, M. Santelli, *Synthesis* **2009**, *6*, 1021–1035.
[31] a) P. Espinet, A. M. Echavarren, *Angew. Chem.* **2004**, *116*, 4808–4839; *Angew. Chem. Int. Ed.* **2004**, *43*, 4704–4734; b) M. Pérez-Rodríguez, A. A. C. Braga, M. Garcia-Melchor, M. H. Pérez-Temprano, J. A. Casares, G. Ujaque, A. R. Lera, R. Alvarez, F. Maseras, P. Espinet, *J. Am. Chem. Soc.* **2009**, *131*, 3650–3657.
[32] CCDC-882425 ((*S*,*S*)-**5a**), 882426 ((*S*,*S*)-**5b**), and 882427 ((*S*,*S*)-**22**) contain the supplementary crystallographic data for this paper. These data can be obtained free of charge from The Cambridge Crystallographic Data Centre via www.ccdc.cam.ac.uk/data_request/cif.
[33] Gaussian 09, Revision A.02, M. J. Frisch, G. W Trucks, H. B. Schlegel, G. E Scuseria, M. A. Robb, J. R Cheeseman, G. Scalmani, V. Barone, B. Mennucci, G. A. Petersson, H. Nakatsuji, M. Caricato, X. Li, H. P Hratchian, A. F. Izmaylov, J. Bloino, G. Zheng, J. L. Sonnenberg, M. Hada, M. Ehara, K. Toyota, R. Fukuda, J. Hasegawa, M. Ishida, T. Nakajima, Y. Honda, O. Kitao, H. Nakai, T. Vreven, J. A. Montgomery, Jr., J. E. Peralta, F. Ogliaro, M. Bearpark, J. J. Heyd, E. Brothers, K. N. Kudin, V. N. Staroverov, R. Kobayashi, J. Normand, K. Raghavachari, A. Rendell, J. C. Burant, S. S. Iyengar, J. Tomasi, M. Cossi, N. Rega, J. M. Millam, M. Klene, J. E. Knox, J. B. Cross, V. Bakken, C. Adamo, J. Jaramillo, R. Gomperts, R. E. Stratmann, O. Yazyev, A. J. Austin, R. Cammi, C. Pomelli, J. W. Ochterski, R. L. Martin, K. Morokuma, V. G. Zakrzewski, G. A. Voth, P. Salvador, J. J. Dannenberg, S. Dapprich, A. D. Daniels, Ö. Farkas, J. B. Foresman, J. V. Ortiz, J. Cioslowski, D. J. Fox, Gaussian, Inc., Wallingford CT, **2009**.
[34] a) C. Lee, W. Yang, R. G. Parr, *Phys. Rev. B* **1988**, *37*, 785–789; b) A. D. Becke, *J. Chem. Phys.* **1993**, *98*, 5648–5652.
[35] P. J. Hay, W. R. Wadt, *J. Chem. Phys.* **1985**, *82*, 299–311.
[36] a) W. J. Hehre, R. Ditchfield, J. A. Pople, *J. Chem. Phys.* **1972**, *56*, 2257–2261; b) P. C. Hariharan, J. A. Pople, *Theor. Chim. Acta* **1973**, *28*, 213–222.
[37] C. Gonzalez, H. B. Schlegel, *J. Phys. Chem.* **1990**, *94*, 5523–5527.

Received: April 24, 2013
Published online: July 25, 2013

